RSC Advances

PAPER

View Article Online
View Journal | View Issue

Check for updates

Cite this: *RSC Adv.*, 2020, **10**, 38174

Facile construction of a ZIF-67/AgCl/Ag heterojunction *via* chemical etching and surface ion exchange strategy for enhanced visible light driven photocatalysis†

Wei Shao,[ac] Yan-Ru Chen,[b] Feng Xie,[a] Hao Zhang,[a] Hai-Tao Wang[bc] and Na Chang *[ac]

Received 8th August 2020
Accepted 5th October 2020

DOI: 10.1039/d0ra06842j

rsc.li/rsc-advances

It is of great importance to design and fabricate heterojunction photocatalysts to improve photocatalytic performance. In this work, a novel ZIF-67/AgCl/Ag heterojunction photocatalyst was successfully synthesized by a facile chemical etching, deposition–precipitation, light-induced reduction approach. After chemical etching by a $AgNO_3$ precursor, the crystal size of ZIF-67 decreased remarkably together with the replacement of Co^{2+} in the framework of ZIF-67 by Ag^+ *via* surface ion exchange. As a result, optical and electrochemical measurements indicated that the separation efficiency of light-induced electrons and holes obviously increased due to the formation of a ZIF-67/AgCl/Ag heterojunction and the surface plasmon resonance of Ag^0. Meanwhile, the corresponding kinetic rate constant of ZIF-67/AgCl/Ag was estimated to be 0.1615 min^{-1}, which was 17, 7.76 and 2.67 times as high as that of individual ZIF-67, AgCl and ZIF-67/AgCl, respectively. The ZIF-67/AgCl/Ag photocatalyst also exhibited good stability and reusability in the process of photodegradation. This work demonstrated a high efficiency photocatalyst for providing new sights into the preparation of a highly efficient MOF-based heterojunction photocatalyst and its potential applications in water purification.

Open Access Article. Published on 16 October 2020. Downloaded on 12/10/2025 2:51:20 PM.
This article is licensed under a Creative Commons Attribution-NonCommercial 3.0 Unported Licence.

1. Introduction

Metal–organic frameworks (MOFs), new types of crystalline and porous materials built from organic ligands and inorganic metal ions, have attracted much attention in the past decades.[1–3] With well-defined structures, high porosity and tunable pore sizes, MOFs have great potential in a diverse range of applications, including gas separation, gas storage, sensing and heterogeneous catalysis.[4–6] Particularly, photoactive MOFs which can absorb visible light and produce photo-induced holes and electrons will further trigger various photo-redox reactions.[7,8] For instance, the Cu-doped ZIF-67 realized the rapid decolorization of MO under visible light illumination[9] and MOF-5 possessed superior visible light reactivity for phenol degradation.[10,11] Although MOFs can absorb in the visible spectrum of solar light, there are still some shortcomings restricting their real application, including the poor separation of photo-induced electron–hole pairs and the high resistance to the transportation of carriers. Thus, it is of great importance to improve the photocatalytic efficiencies of MOFs for meeting the requirements of photocatalysis driven by solar energy.

Recently, as a well-known photosensitive semiconductor with the bandgap of 3.25 eV, AgCl is considered as one of the most widely investigated photocatalyst because of their structural stability.[12,13] Unfortunately, AgCl can be directly excited by ultraviolet (UV) irradiation, which only accounts for about 4% of the solar spectrum. Limited light absorption region often results in the low efficiency of light utilization and slow rate of photochemical process. Therefore, it is important to design suitable photocatalysts for facilitating trapping/absorbing more visible light and achieving better photocatalytic performances. Based on the latest studies, silver/silver halides-based compounds (Ag/AgX, X = Cl, Br, I) have been proved as potential high-efficient photocatalysts, which possess stronger visible light absorption due to the surface plasmon resonance (SPR).[14–16] As an effective strategy for high performance photocatalysis, plasmonic photocatalysis which involves dispersal noble-metal nanoparticles (Au, Ag), obtains remarkable enhancement of photo-reactivity under the irradiation of a broad range of solar light.[17,18]

Herein, we design and fabricate a novel ZIF-67/AgCl/Ag heterojunction photocatalyst *via* a simple chemical etching, surface ion exchange and light-induced reduction strategy. ZIF-

[a]School of Chemistry and Chemical Engineering, Tiangong University, Tianjin 300387, China. E-mail: changna@tiangong.edu.cn; Tel: +86-22-83955622

[b]School of Environmental Science and Engineering, Tiangong University, Tianjin 300387, China

[c]State Key Laboratory of Separation Membrane and Membrane Process, Tianjin 300387, China

† Electronic supplementary information (ESI) available. See DOI: 10.1039/d0ra06842j

This journal is © The Royal Society of Chemistry 2020

Open Access Article. Published on 16 October 2020. Downloaded on 12/10/2025 2:51:20 PM.
This article is licensed under a Creative Commons Attribution-NonCommercial 3.0 Unported Licence.

67 which is considered as a favorable candidate in various photoelectrochemical reactions, exhibits a suitable band gap of about 1.98 eV. Besides, due to the open channels and accessible pores, ZIF-67 possesses regular structure which facilitates the diffusion and adsorption of Ag^+ based reactants in order to potentially overcome the low charge mobility of nonporous semiconductors. After chemical etching and surface ion exchange by $AgNO_3$ precursor, the crystal size of ZIF-67 decreases remarkably without the decomposition of the framework, and the separation efficiency of light-induced charge carriers increases dramatically due to the formation of ZIF-67/AgCl/Ag heterojunction together with the SPR of Ag^0. The crystal structure, morphologies and photocatalytic performances of ZIF-67/AgCl/Ag photocatalyst have been systematically explored. The active species are also investigated, and the possible mechanism of ZIF-67/AgCl/Ag nano-composite is speculated.

2. Experimental

2.1 Materials

$Co(NO_3)_2 \cdot 6H_2O$, $CoCl_2 \cdot 6H_2O$, 2-methylimidazole (2-MIm) and $AgNO_3$ were purchased from Sinopharm Chemical Reagent Co., Ltd. Methanol and isopropyl alcohol (IPA) were purchased from Tianjin Concord Chemical Reagent Co., Ltd. Nafion perfluorinated resin solution (5 wt%) was obtained from Sigma-Aldrich. Ultra-pure water (18.2 MΩ) was prepared by Milli-Q water purification system.

2.2 Sample preparation

2.2.1 Preparation of ZIF-67. ZIF-67 nanocrystals were prepared according to procedures reported previously with some modifications.[19] Typically, $Co(NO_3)_2 \cdot 6H_2O$ (6.489 g) and 2-methylimidazole (1.3686 g) were dissolved methanol (100 mL), respectively, before mixing and stirring at room temperature for 5 h. Purple crystals were collected and washed three times with methanol, and then dried at 60 °C for 10 h.

2.2.2 Preparation of AgCl and AgCl/Ag. Typically, $AgNO_3$ (2 mmol) was dissolved in methanol (30 mL) under stirring at room temperature (solution A). Meanwhile, $CoCl_2 \cdot 6H_2O$ (0.5 mmol) was dissolved in methanol (10 mL) under the same condition (solution B) before introducing to solution A drop by drop in dark under continuous stirring. After 60 min, the white AgCl precipitates were separated, washed by fresh methanol, and dried under vacuum for 10 h. For preparation of AgCl/Ag, the suspension which was formed by the same solution B and solution A was prepared firstly following the same procedure. Subsequently, after stirring for 40 min in dark, the suspension was irradiated under ultraviolet light for another 20 min. Finally, the pale brown AgCl/Ag was separated, washed by fresh methanol, and dried under vacuum for 10 h.

2.2.3 Preparation of ZIF-67/AgCl and ZIF-67/AgCl/Ag. Fig. 1 illustrated the schematic synthesis procedure of ZIF-67/AgCl/Ag. For preparation of ZIF-67/AgCl/Ag photocatalyst, 50 mg of ZIF-67 was added to solution A under continuous stirring in dark for 30 min to form homogeneous suspension. Subsequently, solution B was introduced to the above-mentioned suspension, and kept stirring in dark for 40 min before irradiated under ultraviolet light for another 20 min. For comparison, ZIF-67/AgCl was prepared under same conditions without irradiation of ultraviolet light. The obtained photocatalysts were collected, washed by fresh methanol, and dried under vacuum for 10 h.

2.3 Characterization

The crystal phases of the prepared samples were identified by X-ray diffraction (XRD) patterns (D8 Advance, Bruker). Scanning electron microscopy (SEM, GeminiSEM500, Zeiss, Germany) was used to explore the morphologies of the prepared samples. Chemical states of each element were characterized by X-ray photoelectron spectroscope (XPS) (K-alpha, Thermofisher). UV-vis diffuse reflectance spectra (DRS) were analyzed using UV-vis spectrophotometer (Shimadzu UV-2700). Photoluminescence (PL) spectra were determined using an F380 fluorescence spectrophotometer with excitation at 338 nm.

2.4 Electrochemical measurement

The electrochemical impedance spectroscopy (EIS), transient photocurrent responses and Mott–Schottky measurement were performed by an electrochemical workstation (CHI760E) in a typical three-electrode quartz cell using Pt as counter

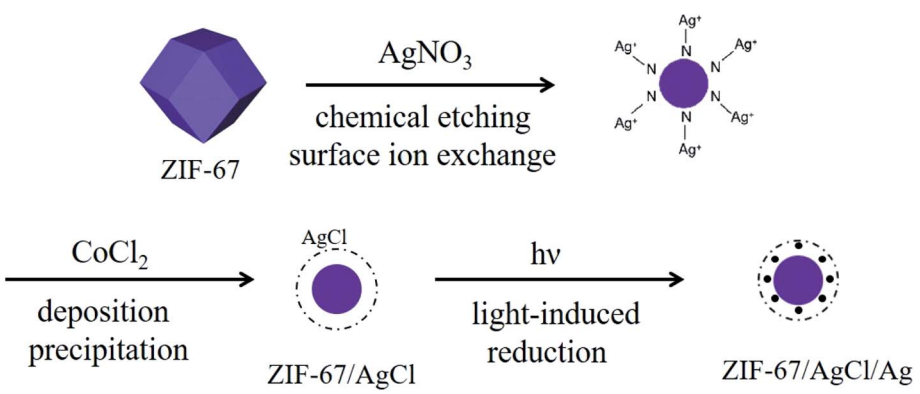

Fig. 1 Schematic illustration of the synthesis procedure of ZIF-67/AgCl/Ag photocatalyst.

Open Access Article. Published on 16 October 2020. Downloaded on 12/10/2025 2:51:20 PM.
This article is licensed under a Creative Commons Attribution-NonCommercial 3.0 Unported Licence.

electrode, saturated calomel electrode (SCE) as reference electrode and modified fluorine-doped tin oxide (FTO) glass as working electrode.

For preparation of the working electrode, 5 mg of the catalyst was mixed with ethanol (1 mL) and Nafion perfluorinated resin solution (10 μL) under ultrasonic condition to form homogeneous solution. 100 μL of the above-mentioned dispersion was deposited onto a FTO glass electrode with coating area of 1 cm^2 for the electrochemical measurements. Finally, the as-prepared catalyst film was dried for 12 h.

Transient photocurrent responses were determined using a 210 W xenon lamp with a 420 nm cutoff filter as light source at a 0.8 V bias voltage potential (*vs.* NHE). EIS tests were conducted under dark circumstance at open circuit potential at the range of frequency between 10^5 and 10^{-2} Hz. The above experiments were carried out in 0.1 M Na_2SO_4 electrolyte solution.

2.5 Photocatalytic performance

The photocatalytic experiments of the photocatalysts were evaluated by decolorization of MO under visible light using a 210 W xenon lamp with a 420 nm cutoff filter. In a typical experiment: 80 mg photocatalyst was added into 120 mL MO aqueous solution (10 mg L^{-1}) in a reactor. In order to reach the adsorption–desorption equilibrium, the suspension was stirred in dark for 30 min prior to further visible light irradiation. The concentration of MO was determined by a UV-vis spectrophotometer.

2.6 Reactive species trapping experiments

Reactive species trapping experiments were performed to clarify the photocatalytic mechanism. The procedure was the same as photocatalytic performance experiment mentioned above except for adding specific scavengers. Typically, $AgNO_3$ (0.5 mmol), 2-MIm (0.5 mmol) and IPA (1 mL) were utilized as e^-, h^+ and ·OH scavengers which were added in the reaction system respectively prior to photocatalytic activity test.

3. Results and discussion

3.1 Characterizations

SEM and TEM images of ZIF-67 and ZIF-67/AgCl/Ag were obtained to show the morphology of the photocatalysts (Fig. 2 and S1†). The as-prepared ZIF-67 crystals were uniform in size (Fig. 2A and S1A†) and had cubic or rhombic dodecahedral morphology with well-defined facet, straight edge, smooth surface (Fig. 2B).[20] The average crystal size of as-prepared ZIF-67 was about 360 nm. It had been demonstrated that MOF crystals could be random etching by H^+, resulting in changing of crystal morphology and decreasing of crystal size.[20–22] After etching by the weak acidic $AgNO_3$ solution and precipitating with the additional Cl^- subsequently, the resulted ZIF-67/AgCl/Ag photocatalyst were still uniform in size and shape (Fig. 2C). However, as shown in Fig. 2D, the as-prepared ZIF-67/AgCl/Ag which changed into spherical morphology possessed obviously smaller particle size (about 60 nm in average) compared to original ZIF-67 (Fig. 2D and S1B†). It was supposed that the original ZIF-67 had been etched by the weak acidic $AgNO_3$–methanol solution (pH = 6.5) and further turn the crystalline ZIF-67 into smaller size. The above results were in accordance with that reported by Meng *et al.*[23]

The crystallinity of as-synthesized crystals was determined by XRD. As shown in Fig. 3A, the XRD patterns of ZIF-67 were in

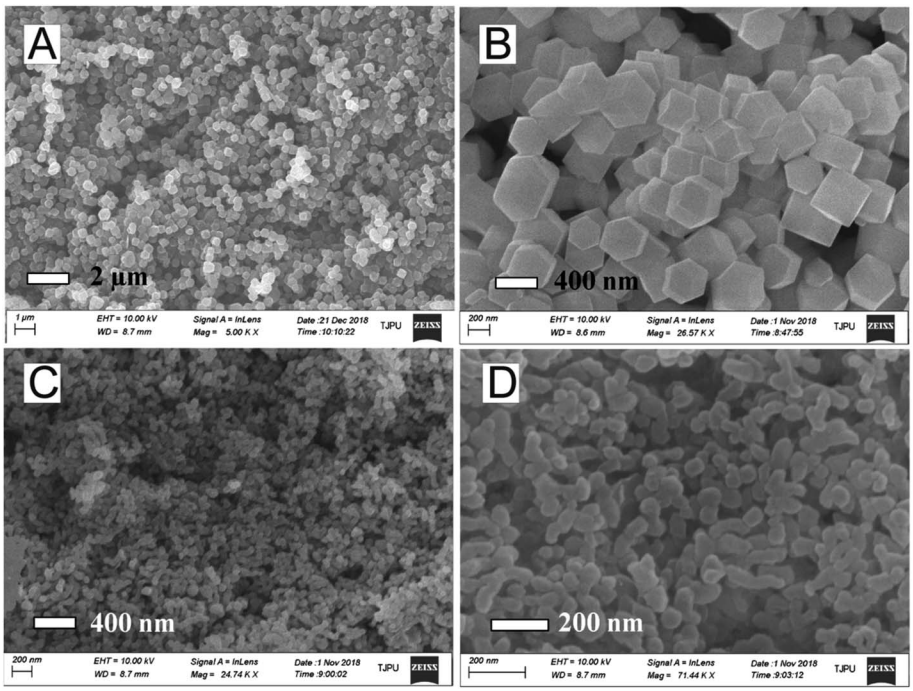

Fig. 2 SEM images of (A and B) ZIF-67 and (C and D) ZIF-67/AgCl/Ag.

 This journal is © The Royal Society of Chemistry 2020

Open Access Article. Published on 16 October 2020. Downloaded on 12/10/2025 2:51:20 PM.
This article is licensed under a Creative Commons Attribution-NonCommercial 3.0 Unported Licence.

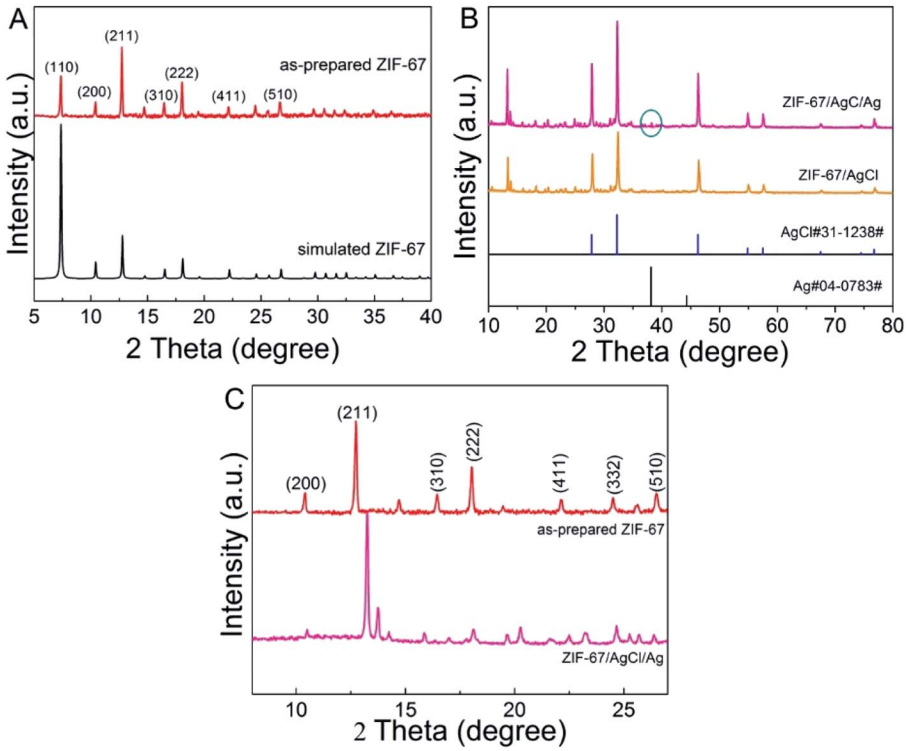

Fig. 3 XRD patterns of (A) as-prepared ZIF-67 and simulated ZIF-67; (B) ZIF-67/AgCl/Ag, ZIF-67/AgCl, standard AgCl and Ag; (C) as-prepared ZIF-67 and ZIF-67/AgCl/Ag.

agreement with simulated ZIF-67 (CCDC-671073), confirming the successful formation of ZIF-67 crystalline. As shown in Fig. 3B, the resulted ZIF-67/AgCl and ZIF-67/AgCl/Ag showed highly strong diffraction peaks at 27.8°, 32.2°, 46.2°, 54.8°, 57.5°, 67.5°, 74.5° and 76.7° which were attributed to the (111), (200), (220), (311), (222), (400), (331) and (420) crystal planes of

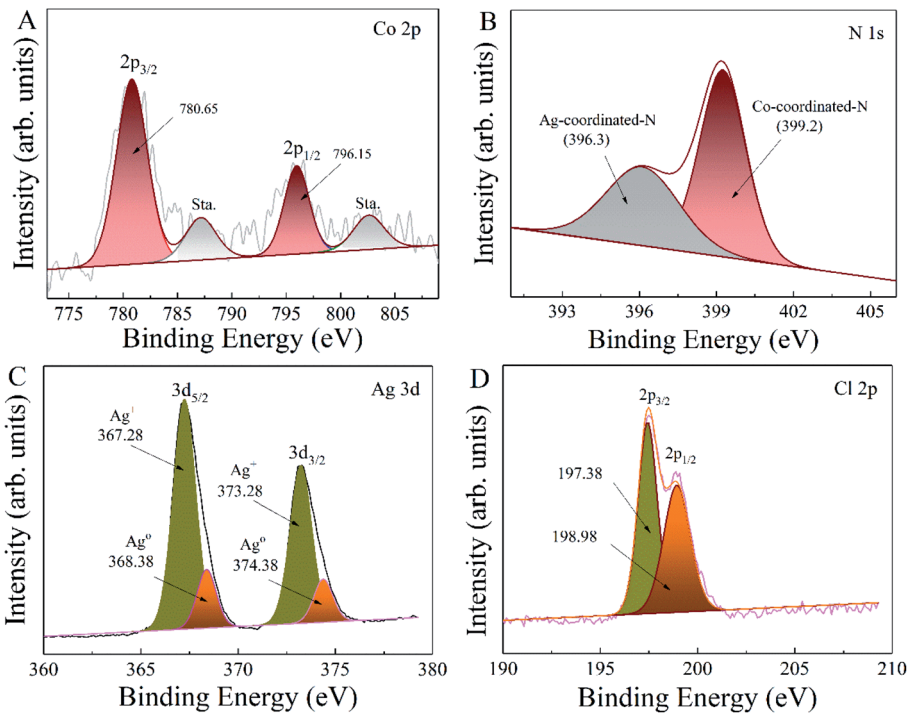

Fig. 4 XPS spectra of ZIF-67/AgCl/Ag (A) Co 2p; (B) N 1s; (C) Ag 3d and (D) Cl 2p.

Open Access Article. Published on 16 October 2020. Downloaded on 12/10/2025 2:51:20 PM.
This article is licensed under a Creative Commons Attribution-NonCommercial 3.0 Unported Licence.

AgCl (JCPDS no. 85-1355). Besides, the as-synthesized ZIF-67/AgCl/Ag also possessed weak peaks around the diffraction angle of 38.1° which was ascribed to the metallic Ag^0 (JCPDS no. 87-717). It was worth to be mentioned that the agreement of XRD patterns between ZIF-67/AgCl/Ag and ZIF-67/AgCl indicated the stability of ZIF-67/AgCl under UV light irradiation, and the formation of Ag^0 by photo-reduction did not change the crystal phase and crystallinity of ZIF-67/AgCl. Moreover, after etching by $AgNO_3$, diffraction peaks originated from ZIF-67 crystals in ZIF-67/AgCl and ZIF-67/AgCl/Ag were obviously weaker than that of AgCl. From the enlarge view of XRD patters shown in Fig. 3C, the main peaks located in (200), (211), (310), (222), (411), (322) and (510) crystal facets of ZIF-67 were still preserved with the diffraction peak corresponding to (211) facets of ZIF-67 in ZIF-67/AgCl/Ag composites shifted to higher angles, which could be attributed to the reduced interlayer spacing.[24] It was possibly originated from the entrance of excessive Ag^+ to the crystal lattice and the subsequently substitution of a great deal of Co^{2+} (ref. 25) which would further confirm by the changing of color from purple (ZIF-67) to gray (ZIF-67/AgCl) and brown (ZIF-67/AgCl/Ag).

XPS was utilized for further analyzing chemical composition and valence states of the as-synthesized ZIF-67/AgCl/Ag and ZIF-67, and the bonding energies were calibrated by the C 1s peak at 284.6 eV. The narrow-scan spectra of the Co 2p, N 1s, Ag 3d and Cl 2p were shown in Fig. 4. The high-resolution spectrum of Co 2p (Fig. 4A) was divided into two main peaks at 780.7 eV and 796.2 eV, corresponding to Co $2p_{3/2}$ and Co $2p_{1/2}$, respectively, and the two satellite peaks of Co $2p_{3/2}$ and Co $2p_{1/2}$ were located at 787.2 eV and 802.5 eV, respectively. The energy gap between the main peak and the satellite peak of Co 2p was further used for determination of the chemical state of Co.[26] The energy gap of Co(II) was corresponded to *ca.* 6.0 eV, while Co(III) was *ca.* 9–10 eV.[27] The results shown above revealed that Co(II) was the main form that existed in the as-prepared ZIF-67/AgCl/Ag, and the chemical etching of $AgNO_3$ together with the photo-reduction from Ag^+ to Ag^0 did not change the chemical state of Co(II) in ZIF-67. However, from the results shown in Fig. 4B, the N 1s spectrum of ZIF-67/AgCl/Ag could obviously be divided into two peaks which located at 399.2 eV and 396.3 eV, respectively. The former peak with relatively higher bonding energy was attributed to the Co–N bond, meanwhile the other peak with lower bonding energy which located at 396.3 eV was attributed to the combination of Ag^+ and N. These results revealed that, except for the Co–N coordination bond which originated from ZIF-67 material, a new Ag–N coordination bond was formed after ZIF-67 etching by $AgNO_3$ and further ion exchanging of Co^{2+} by Ag^+ in the ZIF-67 crystal lattice. The results shown in N 1s spectrum were completely in accordance with the results shown in XRD analysis. The Ag 3d region in Fig. 4C were fitted into two peaks at 367.7 eV and 373.7 eV, which were ascribed to Ag $3d_{5/2}$ and Ag $3d_{3/2}$, respectively. These two peaks could be further divided into four different peaks located at 367.28 eV, 368.38 eV as well as 373.28 eV and 374.38 eV. Bonding energies at 367.28 eV and 373.28 eV were attributed to the Ag^+, while peaks at 368.38 eV and 374.38 eV were ascribed to the metallic Ag^0. These results further proved the co-existence of metallic Ag^0 in ZIF-67/AgCl/Ag photocatalyst. The peaks of the Cl 2p were centered at 198.98 eV and 197.38 eV,

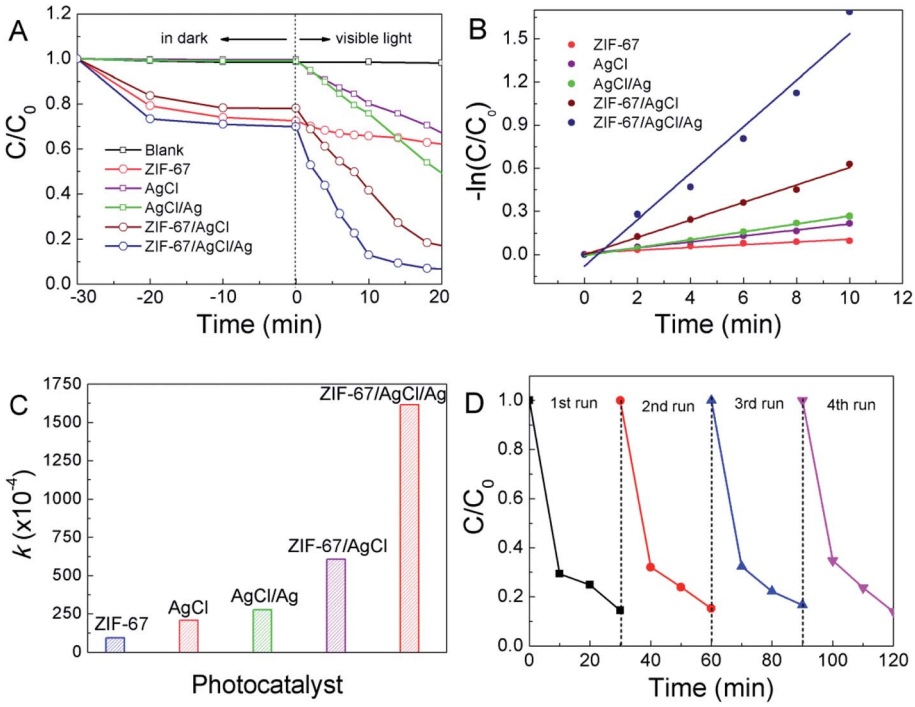

Fig. 5 Photocatalytic performance of the as-prepared samples under visible light irradiation: (A) adsorption and photocatalytic degradation curves; (B) model of pseudo-first order kinetics; (C) the apparent reaction rate constants (*k*) and (D) the reusability of ZIF-67/AgCl/Ag photocatalyst and the recycling run in the photocatalytic reaction.

 This journal is © The Royal Society of Chemistry 2020

Open Access Article. Published on 16 October 2020. Downloaded on 12/10/2025 2:51:20 PM.
This article is licensed under a Creative Commons Attribution-NonCommercial 3.0 Unported Licence.

which were ascribed to Cl $2p_{1/2}$ and Cl $2p_{3/2}$ deriving from Cl^- of AgCl (Fig. 4D).

3.2 Photocatalytic performance

The adsorption and photocatalytic activities of the photocatalysts were evaluated by decomposition of MO under visible light illumination after reaching to the adsorption–desorption equilibrium at the first 30 min in dark (Fig. 5A and S2†). As a result, ZIF-67/AgCl and ZIF-67/AgCl/Ag exhibited obviously higher adsorption capacity than AgCl and AgCl/Ag because of the co-existence of porous ZIF-67 framework, showing the MO removing efficiency of 22% and 30% for ZIF-67/AgCl and ZIF-67/AgCl/Ag, respectively. It was worth to mentioned that the adsorption capacity of ZIF-67/AgCl/Ag was almost equal to the original ZIF-67, though the BET surface area of ZIF-67/AgCl/Ag (1108 $cm^3\ g^{-1}$) was smaller than ZIF-67 (1283 $cm^3\ g^{-1}$) (Fig. S3†). On account of the combination of AgCl/Ag and ZIF-67, ZIF-67/AgCl/Ag possessed better adsorption capacity and photocatalytic activity, and the total organic carbon (TOC) removing ratio was up to 76.5% after 60 min (Fig. S4†). Furthermore, to obtain the photocatalytic activities of each sample, the following pseudo-first-order kinetics model was used: $-\ln(C/C_0) = kt$, where C_0 (mg L^{-1}) is the initial concentration of MO, C (mg L^{-1}) is the concentration of MO at reaction time t (min) and the slope k is the apparent reaction rate constant (min^{-1}).[28,29] As shown in Fig. 5B, ZIF-67/AgCl/Ag revealed the highest photocatalytic activity compared to the other samples. The k values of each photocatalyst calculated from the slopes of the kinetic plots were shown in Fig. 5C. The corresponding kinetic rate constant of ZIF-67/AgCl/Ag was 0.1615 min^{-1}, which was 17, 7.76 and 2.67 times as high as that of individual ZIF-67, AgCl and ZIF-67/AgCl, respectively.

3.3 Stability and reusability

Stability of the catalyst was crucial in practical catalytic process, thus, the reusability of ZIF-67/AgCl/Ag photocatalyst had been investigated. Recycling was achieved by centrifugation for separation of the catalyst, followed by multiple washing with ethanol before drying in vacuum. As shown in Fig. 5D, the photocatalytic activity of ZIF-67/AgCl/Ag did not obviously reduce after testing for four recycles, suggesting the high stability of ZIF-67/AgCl/Ag photocatalyst.

3.4 Optical and electrochemical properties

In order to further reveal the intrinsic features of ZIF-67/AgCl/Ag for the improvement in photocatalytic activity, optical and electrochemical properties were systematically investigated. UV-vis DRS of AgCl, ZIF-67, ZIF-67/AgCl and ZIF-67/AgCl/Ag photocatalyst were shown in Fig. 6 to show the optical absorption ability. For the AgCl photocatalyst, the signature absorption was mainly located at UV region below the wavelength of 400 nm. In the coordination state of ZIF-67 between Co(II) ions and 2-methylimidazole ligand, three visible absorption peaks (537, 565, and 590 nm) were displayed, which could be assigned to $^4A_2(F) \rightarrow {}^4T_1(P)$ transition of Co(II) ions in tetrahedral environments, that was the spin coupling triple peaks.[27,30] It was worth to mention that the ZIF-67/AgCl showed obviously stronger visible light absorption intensity ranging from 400 nm to 760 nm after the introduction of ZIF-67. It might be originated from the effect of interface between ZIF-67 and AgCl, and the cation exchange of Co^{2+} by Ag^+. Furthermore, the ZIF-67/AgCl/Ag photocatalyst exhibited the strongest optical absorption centered at 475 nm in visible light region, which was attributed to SPR effect of Ag nanoparticles,[31] together with the powder color changing from grey to brown because of the formation of Ag^0. The enhanced absorption of visible light would provide ZIF-67/AgCl/Ag photocatalyst with more opportunity to produce more active species for driving the photocatalytic reaction and resulting higher photocatalytic efficiency. Besides, the band gaps of AgCl and ZIF-67 were also estimated according to the UV-DRS spectra, and the corresponding band gap values (E_g) were 2.99 eV and 1.92 eV for AgCl[32] and ZIF-67, respectively.

Furthermore, the transfer and separation behaviors of photo induced charge carriers were investigated to explore improvement of photocatalytic activity on the basis of the PL spectra at the excitation wavelength of 338 nm.[33–35] As shown in Fig. 7, the observed PL intensity of ZIF-67/AgCl/Ag was much weaker than the other photocatalyst, revealing that ZIF-67/AgCl/Ag had longer lifetime of electron–hole pairs because of surface plasma resonance of Ag^0. Besides, recombination of photo-induced electron–hole pairs of ZIF-67/AgCl/Ag was extremely inhibited due to surface heterojunction structure between ZIF-67 and AgCl/Ag, which would lead to a higher photocatalytic activity

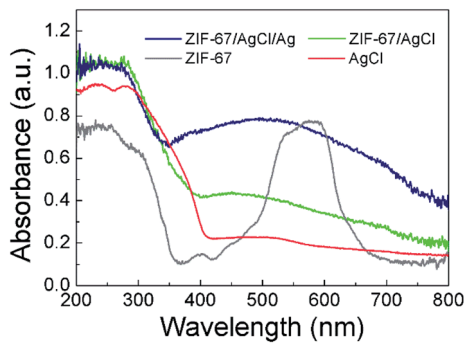

Fig. 6 UV-DRS spectra of the as-prepared photocatalysts.

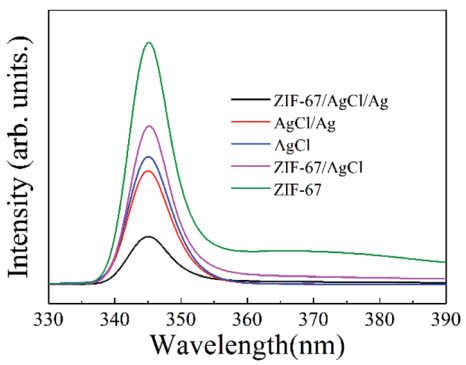

Fig. 7 PL emission spectra of the as-prepared photocatalysts.

Open Access Article. Published on 16 October 2020. Downloaded on 12/10/2025 2:51:20 PM.
This article is licensed under a Creative Commons Attribution-NonCommercial 3.0 Unported Licence.

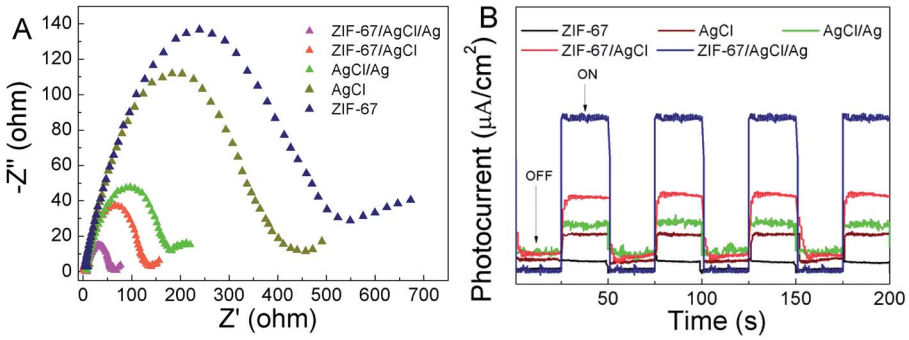

Fig. 8 (A) EIS spectroscopy and (B) transient photocurrent response of the as-prepared samples.

compare to other photocatalyst. Nevertheless, ZIF-67/AgCl showed higher PL intensity compared to AgCl and AgCl/Ag, which would go against the improvement of photocatalytic activity.

Furthermore, EIS analysis and the photocurrent measurements were also performed to examine charge transfer and separation behaviors. The Nyquist plot of EIS was displayed in Fig. 8A, and a smaller radius of Nyquist arc indicated a better electronic conductivity and charge transfer performance. It was found that the ZIF-67/AgCl/Ag has lowest radius of Nyquist arc comparing with ZIF-67/AgCl, AgCl and ZIF-67. The lowest electron transfer resistance attributed to coupling of ZIF-67 and AgCl/Ag and the SPR effect of Ag^0, which facilitated the separation of photo-induced carriers and improved the photocatalytic efficiency. The transient photocurrent responses were recorded for four off–on cycles under dark or visible light irradiation conditions. As shown in Fig. 8B, the photocurrent density of ZIF-67/AgCl/Ag was the highest among the other photocatalysts, which agreed with the sequence of photocatalytic activity. The SPR effect of Ag^0 and the synergistic effect between ZIF-67 and AgCl/Ag efficiently inhibited the recombination of photo-induced carriers and accelerated the rapid charge transfer through Ag^0.

3.5 Reactive species trapping experiments

To further identify the active species generated by ZIF-67/AgCl/Ag during photocatalysis process, trapping experiments were used. In this work, $AgNO_3$, 2-MIm and IPA were utilized as e^-, h^+ and ·OH scavengers, respectively. As shown in Fig. 9, the photocatalytic degradation rates were obviously prohibited when $AgNO_3$ and IPA were used as scavengers, suggesting that e^- and ·OH radical were the major reactive species in ZIF-67/AgCl/Ag photocatalytic reaction system. However, when 2-MIm was introduced as the h^+ scavenger, the photocatalytic degradation rate was seldom inhibited, indicating that h^+ was not the major reactive species in this reaction system.

3.6 Mott–Schottky measurement and possible photocatalytic mechanism

To further illustrate the possible reason for the higher photocatalytic activity based on the ZIF-67/AgCl/Ag photocatalyst and reveal the photocatalytic mechanism, Mott–Schottky (M–S) curves were employed for elucidating the band energy potentials. As shown in Fig. 10, the positive slopes of these plots revealed that AgCl and ZIF-67 were n-type semiconductors,[36] and flat band potential (E_{fb}) of ZIF-67 and AgCl were calculated to be −0.98 eV (*vs.* SCE) and −0.82 eV (*vs.* SCE), respectively. Herein, the conduction band (CB) potential (E_{cb}) of ZIF-67 and AgCl were −0.74 eV (*vs.* NHE) and −0.58 eV (*vs.* NHE), respectively. The relative valence band (VB) potential (E_{vb}) of ZIF-67 and AgCl were 1.18 eV and 2.41 eV, which were calculated by equation of $E_{vb} = E_{cb} + E_g$.

Base on the results shown above, the mechanism for the enhanced photocurrent and photocatalysis reaction was

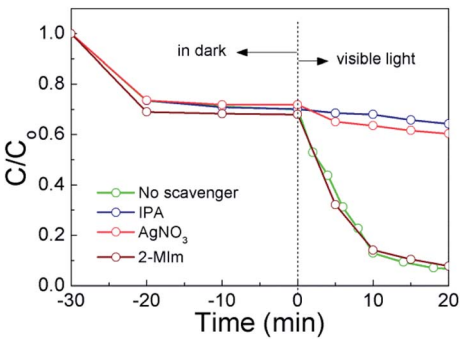

Fig. 9 Effect of different scavengers on the photodegradation of MO by ZIF-67/AgCl/Ag photocatalyst under visible light irradiation.

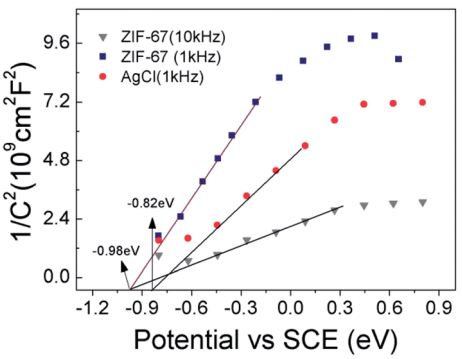

Fig. 10 The Mott–Schottky plots of the as-prepared samples.

This journal is © The Royal Society of Chemistry 2020

Open Access Article. Published on 16 October 2020. Downloaded on 12/10/2025 2:51:20 PM.
This article is licensed under a Creative Commons Attribution-NonCommercial 3.0 Unported Licence.

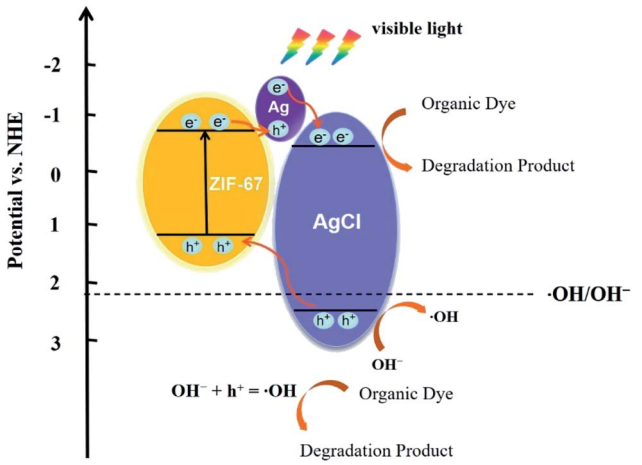

Fig. 11 Proposed photocatalytic mechanism of the ZIF-67/AgCl/Ag photocatalyst.

proposed and illustrated in Fig. 11. Except for the photo-induced electrons excited from the VB to the CB of AgCl under visible light irradiation, the SPR-excited electrons of Ag^0 also transported to the CB of AgCl through Ag–AgCl interfaces,[7] which would further facilitate the photo-decomposition of MO. Meanwhile, due to the low band gap energy of 1.92 eV, ZIF-67 could be easily excited under visible light, and the electrons were transformed from VB of ZIF-67 to its CB. The photo-generated electrons from excited ZIF-67 were simultaneously recombined with the left positive charge species in Ag region, while the holes from the VB of ZIF-67 were transferred to the VB of AgCl.[37,38] The separation efficiency of photo-induced carriers in ZIF-67 was effectively promoted, resulting in more free electrons in the CB of AgCl. Furthermore, the VB potential of AgCl was higher than the redox potential of ·OH/OH^- (2.38 eV *vs.* NHE), and ·OH radicals was generated by oxidation of OH^- by h^+ which would further trigger the redox reactions.

4. Conclusions

A novel ZIF-67/AgCl/Ag heterojunction photocatalyst were successfully synthesized using a simple chemical etching and deposition–precipitation method with Ag^0 introduced by light-induced reduction from Ag^+. Due to smaller crystal sizes of the ZIF-67/AgCl/Ag heterojunction and the SPR effect of Ag^0, the separation efficiency of photo-induced carriers increases which resulted to a higher photocatalytic efficiency of ZIF-67/AgCl/Ag heterojunction photocatalyst compared to pure ZIF-67, ZIF-67/AgCl, AgCl and AgCl/Ag. The ZIF-67/AgCl/Ag photocatalyst exhibited stability and reusability in the process of photo-degradation. The active species in the ZIF-67/AgCl/Ag photocatalytic reaction system were also investigated, and e^- and ·OH radical were the major reactive species. In summary, this work demonstrated a high efficiency photocatalyst for providing new sights into the preparation of MOF-based photocatalyst and potential applications in water purification.

Conflicts of interest

There are no conflicts to declare.

Acknowledgements

This work was supported by National Key R&D Program of China (2019YFC0408401, 2019YFC0408404), Postdoctor Science Foundation of China (2018M630275), Tianjin Key Science and Technology Program Foundation (18ZXSZSF00010, 19YFSLQY00060, 19PTZWHZ00030).

References

1 K. Shen, L. Zhang, X. D. Chen, L. M. Liu, D. L. Zhang, Y. Han, J. Y. Chen, J. L. Long, L. Rafael, Y. W. Li and B. L. Chen, Ordered macro-microporous metal-organic framework single crystals, *Science*, 2018, **359**, 206–210.
2 Z. R. Herm, B. M. Wiers, J. A. Mason, J. M. van Baten, M. R. Hudson, P. Zajdel, C. M. Brown, N. Masciocchi, R. Krishna and J. R. Long, Separation of Hexane Isomers in a Metal-Organic Framework with Triangular Channels, *Science*, 2013, **340**, 960–964.
3 P. G. Boyd, A. Chidambaram, E. García-Díez, C. P. Ireland, T. D. Daff, R. Bounds, A. Gladysiak, P. Schouwink, S. M. Moosavi, M. M. Maroto-Valer, J. A. Reimer, J. A. R. Navarro, T. K. Woo, S. Garcia, K. C. Stylianou and B. Smit, Data-driven design of metal-organic frameworks for wet flue gas CO_2 capture, *Nature*, 2019, **576**, 253–256.
4 J. Zheng, X. Cui, Q. Yang, Q. Ren, Y. Yang and H. Xing, Shaping of ultrahigh-loading MOF pellet with a strongly anti-tearing binder for gas separation and storage, *Chem. Eng. J.*, 2018, **354**, 1075–1082.
5 Z. K. Wang, L. Ge, M. R. Li, R. J. Lin, H. Wang and Z. H. Zhu, Orientated growth of copper-based MOF for acetylene storage, *Chem. Eng. J.*, 2019, **357**, 320–327.
6 B. N. Bhadra, A. Vinu, C. Serre and S. H. Jhung, MOF-derived carbonaceous materials enriched with nitrogen: Preparation and applications in adsorption and catalysis, *Mater. Today*, 2019, **25**, 88–111.
7 Q. Liu, C. Zeng, L. Ai, Z. Hao and J. Jiang, Boosting visible light photoreactivity of photoactive metal-organic framework: Designed plasmonic Z-scheme Ag/AgCl@MIL-53-Fe, *Appl. Catal., B*, 2018, **224**, 38–45.
8 N. Liu, W. Huang, X. Zhang, L. Tang, L. Wang, Y. Wang and M. Wu, Ultrathin graphene oxide encapsulated in uniform MIL-88A(Fe) for enhanced visible light-driven photodegradation of RhB, *Appl. Catal., B*, 2018, **221**, 119–128.
9 H. Yang, X. W. He, F. Wang, Y. Kang and J. Zhang, Doping copper into ZIF-67 for enhancing gas uptake capacity and visible-light-driven photocatalytic degradation of organic dye, *J. Mater. Chem.*, 2012, **22**, 21849–21851.
10 F. Xamena, A. Corma and H. Garcia, Applications for metal−organic frameworks (MOFs) as quantum dot semiconductors, *J. Phys. Chem. C*, 2007, **111**, 80–85.

Open Access Article. Published on 16 October 2020. Downloaded on 12/10/2025 2:51:20 PM.
This article is licensed under a Creative Commons Attribution-NonCommercial 3.0 Unported Licence.

11 C. G. Silva, A. Corma and H. García, Metal–organic frameworks as semiconductors, *J. Mater. Chem.*, 2010, **20**, 3141–3156.

12 D. Xu, W. Shi, C. Song, M. Chen, S. Yang, W. Fan and B. Chen, In-situ synthesis and enhanced photocatalytic activity of visible-light-driven plasmonic Ag/AgCl/$NaTaO_3$ nanocubes photocatalysts, *Appl. Catal., B*, 2016, **191**, 228–234.

13 D. Sun, Y. Zhang, Y. Liu, Z. Wang, X. Chen, Z. Meng, S. Kang, Y. Zheng, L. Cui and M. Chen, In-situ homodispersely immobilization of Ag@AgCl on chloridized g-C_3N_4 nanosheets as an ultrastable plasmonic photocatalyst, *Chem. Eng. J.*, 2020, **384**, 123259.

14 Y. Fan, W. Ma, D. Han, S. Gan, X. Dong and L. Niu, Convenient recycling of 3D AgX/graphene aerogels (X= Br, Cl) for efficient photocatalytic degradation of water pollutants, *Adv. Mater.*, 2015, **27**, 3767–3773.

15 J. J. Yu, D. P. Sun, T. H. Wang and F. Li, Fabrication of Ag@AgCl/ZnO submicron wire film catalyst on glass substrate with excellent visible light photocatalytic activity and reusability, *Chem. Eng. J.*, 2018, **334**, 225–236.

16 N. M. Mahmoodi, A. Taghizadeh, M. Taghizadeh and J. Abdi, In situ deposition of Ag/AgCl on the surface of magnetic metal-organic framework nanocomposite and its application for the visible-light photocatalytic degradation of Rhodamine dye, *J. Hazard. Mater.*, 2019, **378**, 120741.

17 X. Yu, F. Liu, J. Bi, B. Wang and S. Yang, Improving the plasmonic efficiency of the Au nanorod-semiconductor photocatalysis toward water reduction by constructing a unique hot-dog nanostructure, *Nano Energy*, 2017, **33**, 469–475.

18 J. Yang and C. Y. Mou, Ordered mesoporous Au/TiO_2 nanospheres for solvent-free visible-light-driven plasmonic oxidative coupling reactions of amines, *Appl. Catal., B*, 2018, **231**, 283–291.

19 W. T. Koo, S. Yu, S. J. Choi, J. S. Jang, J. Y. Cheong and I. D. Kim, Nanoscale PdO catalyst functionalized Co_3O_4 hollow nanocages using MOF templates for selective detection of acetone molecules in exhaled breath, *ACS Appl. Mater. Interfaces*, 2017, **9**, 8201–8210.

20 C. Avci, J. Ariñez-Soriano, A. Carné-Sánchez, V. Guillerm, C. Carbonell, I. Imaz and D. Maspoch, Post-Synthetic Anisotropic Wet-Chemical Etching of Colloidal Sodalite ZIF Crystals, *Angew. Chem.*, 2015, **127**, 14625–14629.

21 M. Hu, A. A. Belik, M. Imura and Y. Yamauchi, Tailored design of multiple nanoarchitectures in metal-cyanide hybrid coordination polymers, *J. Am. Chem. Soc.*, 2013, **135**, 384–391.

22 Y. Yoo and H. K. Jeong, Generation of covalently functionalized hierarchical IRMOF-3 by post-synthetic modification, *Chem. Eng. J.*, 2012, **181**, 740–745.

23 W. Meng, Y. Wen, L. Dai, Z. He and L. Wang, A novel electrochemical sensor for glucose detection based on Ag@ZIF-67 nanocomposite, *Sens. Actuators, B*, 2018, **260**, 852–860.

24 Y. Zhang and S. J. Park, Facile construction of MoO_3@ZIF-8 core-shell nanorods for efficient photoreduction of aqueous Cr(VI), *Appl. Catal., B*, 2019, **240**, 92–101.

25 H. T. Wang, Y. P. Liu, H. Zhang, N. Chang, W. Shao, M. S. Shi, D. Ao and M. C. Lu, Design and synthesis of porous C–ZnO/TiO_2@ ZIF-8 multi-component nano-system via pyrolysis strategy with high adsorption capacity and visible light photocatalytic activity, *Microporous Mesoporous Mater.*, 2019, **288**, 109548.

26 D. Barreca, C. Massignan, S. Daolio, M. Fabrizio, C. Piccirillo, L. Armelao and E. Tondello, Composition and microstructure of cobalt oxide thin films obtained from a novel cobalt(II) precursor by chemical vapor deposition, *Chem. Mater.*, 2001, **13**, 588–593.

27 J. Qin, S. Wang and X. Wang, Visible-light reduction CO_2 with dodecahedral zeolitic imidazolate framework ZIF-67 as an efficient co-catalyst, *Appl. Catal., B*, 2017, **209**, 476–482.

28 C. Li, S. Yu, H. Dong, C. Liu, H. Wu, H. Che and G. Chen, Z-scheme mesoporous photocatalyst constructed by modification of Sn_3O_4 nanoclusters on g-C_3N_4 nanosheets with improved photocatalytic performance and mechanism insight, *Appl. Catal., B*, 2018, **238**, 284–293.

29 H. Dong, X. Zhang, J. Li, P. Zhou, S. Yu, N. Song, C. Liu, G. Che and C. Li, Construction of morphology-controlled nonmetal 2D/3D homojunction towards enhancing photocatalytic activity and mechanism insight, *Appl. Catal., B*, 2020, **263**, 118270.

30 H. Li, H. Ma, X. Wang, J. Gao, C. Chen, S. Shi, M. Qu, N. Feng and J. Xu, Efficient oxidation of ethylbenzene catalyzed by cobalt zeolitic imidazolate framework ZIF-67 and NHPI, *J. Energy Chem.*, 2014, **23**, 742–746.

31 L. Ai, C. Zhang and J. Jiang, Hierarchical porous AgCl@Ag hollow architectures: self-templating synthesis and highly enhanced visible light photocatalytic activity, *Appl. Catal., B*, 2013, **142**, 744–751.

32 H. Yang, X. W. He, F. Wang, Y. Kang and J. Zhang, Doping copper into ZIF-67 for enhancing gas uptake capacity and visible-light-driven photocatalytic degradation of organic dye, *J. Mater. Chem.*, 2012, **22**, 21849–21851.

33 H. Dong, M. Xiao, S. Yu, H. Wu, Y. Wang, J. Sun, G. Chen and C. Li, Insight into the Activity and Stability of Rh_xP Nano-Species Supported on g-C_3N_4 for Photocatalytic H_2 Production, *ACS Catal.*, 2020, **10**, 458–462.

34 C. Li, Y. Du, D. Wang, S. Yin, W. Tu, Z. Chen, M. Kraft, G. Chen and R. Xu, Unique P=Co=N Surface Bonding States Constructed on g-C_3N_4 Nanosheets for Drastically Enhanced Photocatalytic Activity of H_2 Evolution, *Adv. Funct. Mater.*, 2017, **27**, 1604328.

35 H. Dong, S. Hong, P. Zhang, S. Yu, Y. Wang, S. Yuan, H. Li, J. Sun, G. Chen and C. Li, Metal-free Z-scheme 2D/2D VdW heterojunction for high-efficiency and durable photocatalytic H_2 production, *Chem. Eng. J.*, 2020, **395**, 125150.

36 H. Huang, K. Xiao, T. Zhang, F. Dong and Y. Zhang, Rational design on 3D hierarchical bismuth oxyiodides via in situ self-template phase transformation and phase-junction

 This journal is © The Royal Society of Chemistry 2020

Open Access Article. Published on 16 October 2020. Downloaded on 12/10/2025 2:51:20 PM.
This article is licensed under a Creative Commons Attribution-NonCommercial 3.0 Unported Licence.

construction for optimizing photocatalysis against diverse contaminants, *Appl. Catal., B*, 2017, **203**, 879–888.

37 J. Zhou, A. Zhou, L. Shu, M. C. Liu, Y. Dou and J. R. Li, Cellular heterojunctions fabricated through the sulfurization of MOFs onto ZnO for high-efficient photoelectrochemical water oxidation, *Appl. Catal., B*, 2018, **226**, 421–428.

38 Y. Li, Y. Fang, Z. Cao, N. Li, D. Chen, Q. Xu and J. Lu, Construction of g-C_3N_4/PDI@MOF heterojunctions for the highly efficient visible light-driven degradation of pharmaceutical and phenolic micropollutants, *Appl. Catal., B*, 2019, **250**, 150–162.